
Article:
Zhou, Nan, Zhang, Cheng, Cao, Yang et al. (4 more authors) (2021) Conversion of xylose into furfural over MC-SnOx and NaCl catalysts in a biphasic system. Journal of Cleaner Production. 127780. ISSN 0959-6526

https://doi.org/10.1016/j.jclepro.2021.127780

Amount of words=7210

Conversion of xylose into furfural over MC-SnO_x and NaCl catalysts in a biphasic system

Nan Zhou[a, b, c, d], Cheng Zhang [d, e], Yang Cao[a, b, c], Jiahui Zhan[a, b, c], Jiajun Fan[f], James H. Clark[a, b, f], Shicheng Zhang[a, b, c, *]

[a] Shanghai Key Laboratory of Atmospheric Particle Pollution and Prevention (LAP3), Department of Environmental Science and Engineering, Fudan University, Shanghai 200438, China.

[b] Shanghai Technical Service Platform for Pollution Control and Resource Utilization of Organic Wastes, Shanghai 200438, China.

[c] Shanghai Institute of Pollution Control and Ecological Security, Shanghai, 200092, China.

[d] These authors contributed equally to this work.

[e] College of Environmental and Resource Sciences, Zhejiang A&F University, Hangzhou 311300, China

[f] Green Chemistry Centre of Excellence, Department of Chemistry, University of York, York, YO10 5DD, UK.

[*]Corresponding author: zhangsc@fudan.edu.cn

ABSTRACT

Furfural is a promising platform chemical that can be catalyzed from lignocellulose biomass. In this study, a novel micro-mesoporous carbon supported tin oxide catalyst (MC-SnO_x) was developed to convert xylose into furfural in a low sodium chloride (NaCl) concentration and acid-free biphasic system. The catalysts synthesized by annealing from 400 °C to 600 °C for 3.5h were characterized by BET, SEM, XPS, XRD, NH_3-TPD and FTIR techniques. The factor that mostly affected the catalytic performance was the acid concentration of the catalysts, and the best catalytic performance was achieved by MC-SnO_x annealed at 450 °C. Further increasing the annealing temperature can cause reduction, volatilization and aggregation of Sn species, which can finally affect acid concentration and performance of the catalyst. In addition, a synergistic catalytic effect was found between MC-SnO_x and NaCl and effectivity of low concentration of NaCl indicated the potential of applying seawater or wastewater containing NaCl as a low-cost reaction solvent and NaCl source. To balance the catalytic performance, cost, equipment safety and environmental concerns, a reasonable furfural yield of 53.9 % was achieved over the MC-SnO_x-450 and NaCl (0.2 M) in biphasic system under mild conditions (180 °C and 20 min) with a good catalyst reusability.

KEYWORDS: Furfural, Annealing temperature, Sn reduction, Xylose conversion, Biphasic solvent, Seawater

Graphical abstract

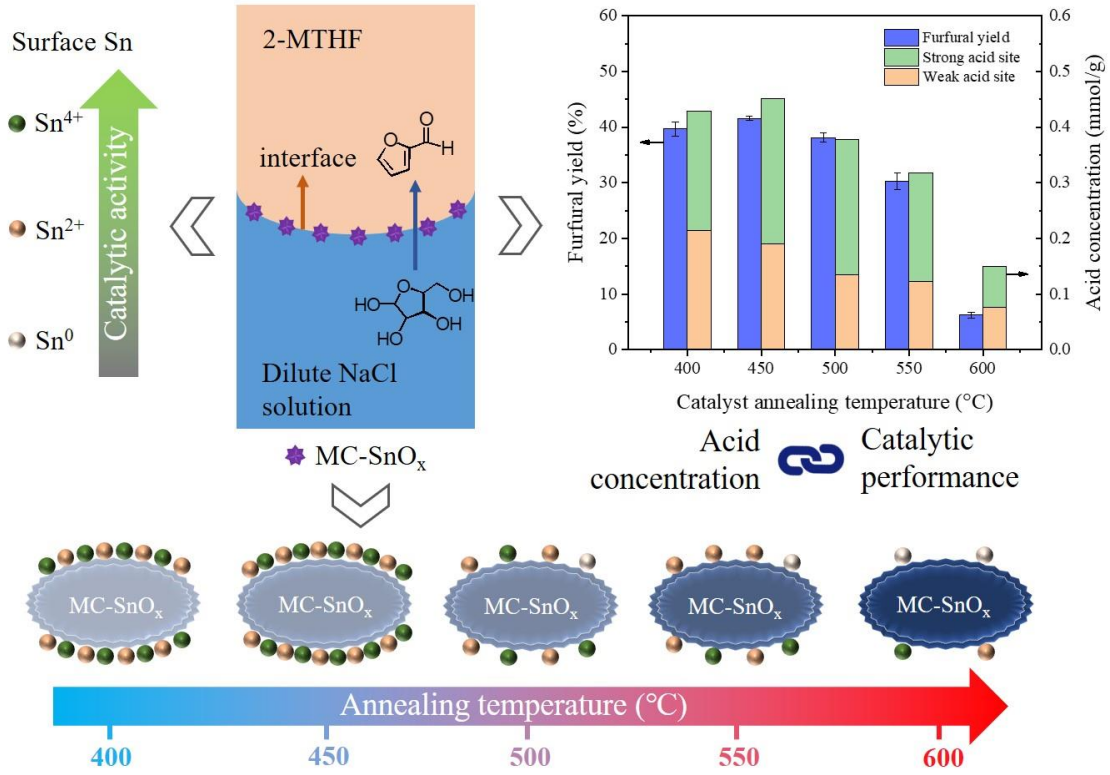

1. Introduction

Furfural is one platform chemical that can be derived from lignocellulose biomass in large scale and can be converted to various useful chemicals to replace part of fossil derived chemicals. Furfural and its conversion products can be used as various industrial raw

47 materials such as resin, adhesives, solvent, biofuel and so on (Bhaumik and Dhepe, 2016).
48 Hence, furfural is believed as a kind of promising bio-based chemical (Wettstein et al.,
49 2012). Currently, furfural is produced by a dilute acid catalytic hydrolysis process in
50 industry. Biomass is first treated with dilute sulfuric acid or hydrochloric acid, and then the
51 furfural is separated by high pressure steam (Choudhary et al., 2012). However, this
52 method is not efficient enough and can produce massive acid wastewater, byproducts and
53 cause severe equipment corrosion (Karinen et al., 2011). To overcome these disadvantages,
54 many catalytic methods were developed to produce furfural.

55 Biphasic solvent systems are often used to enhance furfural yields. With $FeCl_3 \cdot 6H_2O$ and
56 sodium chloride (NaCl) in the aqueous phase and 2-methyltetrahydrofuran (2-MTHF) as
57 the organic phase, a furfural yield of 71% was achieved with 98% furfural extracted
58 (Vomstein et al., 2011). The advantages of the biphasic system are that furfural can be
59 transferred to the organic phase and the reduction in the furfural concentration minimizes
60 the degradation of furfural (Cai et al., 2014). Also, furfural can be recovered from the
61 reaction solvent more easily (Sweygers et al., 2018). Among organic solvents, 2-MTHF
62 displays promising application potential because of its good extraction ability (Wang et al.,
63 2015), low toxicity (Lin et al., 2017), acid stability and recycle convenience (Li et al., 2016).

64 Chloride salts were found to have excellent catalytic efficiency. Researchers studied the
65 catalysis influence of $FeCl_3$, $AlCl_3$, NaCl and HCl on furfural synthesis (Li et al., 2016).

66 $FeCl_3$ showed a similar catalysis effect with HCl in aqueous phase and NaCl also improve
67 the synthesis of furfural when $FeCl_3$, $AlCl_3$ or HCl are in the system. Other salts like $SnCl_4$
68 (Wang et al., 2015), $ZnCl_2$, $MnCl_2$ (Jiang et al., 2018), $CuCl_2$ (Guenic et al., 2015), $CrCl_3$
69 (Choudhary et al., 2012), $Al_2(SO_4)_3$ (Yang et al., 2017) and alkali halide (Enslow and Bell,
70 2015) have been proven to have considerable promotion on furfural production. In addition,
71 the salting out effect of chlorides also contribute to the higher yields due to more product
72 can be extracted by the organic phase (Román-Leshkov et al., 2007). To realize greener
73 conversion, researchers applied seawater to furfural production. However, in previous
74 studies seawater itself cannot provide enough catalytic effect because of its low NaCl
75 concentration. Systems containing concentrated seawater and other homogeneous catalysts
76 were proven effective in xylose conversion into furfural (T. Guo et al., 2018; Vomstein et
77 al., 2011).
78 However, high concentration of chlorides can also cause equipment corrosion at high
79 temperatures. Thus, heterogeneous catalysts have been widely explored in furfural
80 production. Heteropoly acids (X. Guo et al., 2018), polymeric solid catalyst (Agirrezabal-
81 Telleria et al., 2012, 2011), metal oxides (H. Li et al., 2014), zeolites (Zhang et al., 2017)
82 and carbon-based catalysts (Wang et al., 2017) have already been proven to be effective in
83 furfural synthesis. The mechanism of xylose conversion into furfural has already been
84 proposed as following one of 3 pathways (Yang et al., 2017): (1) xylose isomerizes to

85 xylulose intermediate and subsequently dehydrates to furfural, (2) xylose directly
86 dehydrate into furfural and (3) xylose in a stepwise fashion dehydrates to furfural through
87 a dicarbonyl intermediate. The second route is common in the homogeneous reactions
88 catalyzed by strong acid (Nimlos et al., 2006). The third route has been proven in the
89 research on Nb_2O_5 catalysis (Gupta et al., 2017). Among the three routes, the first route is
90 widely accepted in the presence of catalysts with both Brønsted and Lewis acid.
91 Among solid catalysts, tin and its oxide showed promising catalytic abilities and addition
92 of SO_4^{2-} can further promote catalytic performance: SO_4^{2-}/SnO_2^- MMT (montmorillonite)
93 (Qing et al., 2017) showed even higher furfural yield in solvents like toluene, methyl
94 isobutyl ketone (MIBK) and cyclopentyl methyl ether (CPME) with addition of NaCl.
95 SO_4^{2-}/SnO_2-diatomite (Jiang et al., 2018) was also found to have a maximum furfural yield
96 of 68.9% in a γ-valerolactone (γ-GVL)–water system with 15 g/L $ZnCl_2$. Waste like coal
97 fly ash has been considered as a support for catalysts: Researchers (Gong et al., 2019)
98 prepared SO_4^{2-}/SnO_2-AI_2O_3-CFA (coal fly ash) and achieved a good furfural yield of 84.7%
99 in the NH_4Cl-toluene biphasic system. As a kind of carbon-based material, bio-based
100 materials which can be found from food and agriculture waste captured researchers'
101 interest because of their characteristics of eco-friendly and low-cost. Rape pollen was used
102 as raw material to produce SO_4^{2-}/Sn-TRP (treated rape pollen) catalyst (Teng et al., 2020).
103 High performance was observed in a prolonged reaction of xylose to furfural, which

reached a furfural yield of 82.79%. However, the sulfuric acid treatment process can discharge acid wastewater while providing catalytic activity to catalysts. Several recent studies reported the effectiveness of such bio-based/carbon-based tin oxide in biorefinery (Yang et al., 2017, 2019). Rare studies reported the application of carbon-supported tin oxide catalyst in furfural production. Since bio-based/carbon-based support has advantages of eco-friendly and low-cost and tin oxide displays promising performance, a greener bio-based/carbon-based tin oxide catalytic system is still deserved to develop.

In this study, we have prepared a novel mesoporous carbon-supported tin oxide catalyst (MC-SnO_x) without acid treatment process, which has proven to have a reasonable catalytic performance with low concentration of NaCl. Characteristics of acid-free process and potential of applying seawater or wastewater containing NaCl enable greener production of furfural. Comprehensive characterization was conducted to construct the structure-performance relationship between MC-SnO_x catalyst and furfural production. In addition to factors like catalyst loading, NaCl concentration, reaction temperature and time, temperature of catalyst's annealing process impacts most on furfural production. The probable mechanism of Sn species content and contribution variation at different annealing temperature was investigated and a catalytic activity order of Sn species was concluded. Finally, the reusability of MC-SnO_x catalyst was studied and proven good. The results are

meaningful for further development of carbon-supported tin oxide catalysts in furfural production.

2. Materials and methods

2.1. Materials

Furfural (≥99.5%), D-xylose (98%) and D-fructose (99%) were supplied by Aladdin Reagent Corporation. 2-methyltetrahydrofuran (2-MTHF) (≥99%), $SnCl_4 \cdot 5H_2O$ (analytical grade) and NaCl (≥99.5%) were brought from Shanghai Titan Scientific Co., LTD, Sinopharm Chemical Reagent Co., Ltd and Shanghai Dahe Chemicals Co. LTD, respectively. Pluronic P-123 (M_w=5800, $EO_{20}PO_{70}EO_{20}$) and Pluronic F-127 (M_w=2600, $EO_{106}PO_{70}EO_{106}$) were purchased from Sigma Aldrich. All reagents were used without further purification.

2.2. Synthesis of MC-SnO_x catalysts

The synthesis method of MC-SnO_x catalysts refers to previous study (Zhang et al., 2019), and the basic process is shown in Fig. 1. P-123 and F-127 were used as composite template in the preparation. Briefly, 8.7 g $SnCl_4 \cdot 5H_2O$, 2 g fructose, 1 g P-123 and 3 g F-127 were dissolved in 70 mL ultrapure water and stirred at room temperature for 2 h. The solution was then sealed in a stainless reactor with 100 mL polytetrafluoroethylene lining and

heated in the oven at 180 °C for 24 h. The mixture was centrifuged and the residual was washed by ultrapure water to neutral pH value, then residual was dried in oven at 80 °C overnight. The as-prepared samples were annealed at the temperature from 400 °C to 600 °C with a heating rate of 2 °C /min in a tube furnace for 3.5 h in a nitrogen atmosphere. Finally, the MC-SnO_x catalysts was ground and pulverized to 80 mesh before use. In the following sections, MC-SnO_x-X is used to represent catalysts annealed at certain temperature. For example, MC-SnO_x-400 is the MC-SnO_x catalyst annealed at 400 °C.

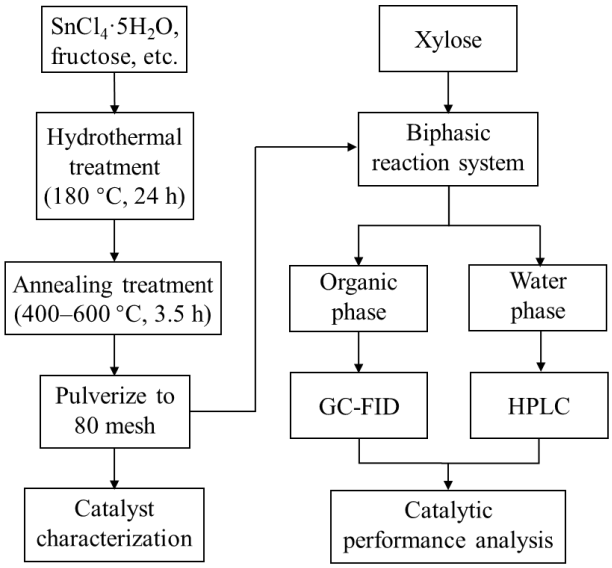

Fig. 1. Diagram of catalyst preparation and furfural production processes

2.3. Conversion of xylose to furfural

As shown in Fig. 1, the catalytic conversion from xylose to furfural was conducted in a 25 mL Hastelloy reactor. A biphasic rate of 1:1 (v/v) was selected because of its prior

153 performance (Qing et al., 2017; Wang et al., 2019). In a typical run, 5 mL aqueous solution
154 containing 20 g/L xylose (some with NaCl) and 5 mL 2-MTHF organic solvent were mixed
155 with MC-SnO_x catalysts in the reactor. Then the reactor was heated up to target temperature
156 (160–180 °C) while stirring at 700 rpm. The reactor can reach the target temperature no
157 longer than 10 min as shown in Fig. S1. When reaction completed, the reactor was cooled
158 in tap water to room temperature quickly. Needle filters equipped with filter paper were
159 used to separate catalysts. Water phase and organic phase was then separate after quick
160 stratification. All samples were filtered by a 0.22 μm syringe filter before analyzing.
161
162 *2.4. Catalysts characterization*
163 Catalysts' specific surface area were analyzed by a Quantachrome Quantasorb SI
164 Brunauer-Emmett-Teller (BET) analyzer. The surface composition and structure of MC-
165 SnO_x catalysts were analyzed by a VEGA3 (TESCAN) scanning electron microscopy
166 (SEM) instrument with a Bruker XFlash Detector 610M energy dispersive spectroscopy
167 (EDS) system. X-ray photoelectron spectroscopy (XPS) was used to analyze the state of
168 the developed catalysts with an RBD-upgraded PHI 5000C ESCA system (Perkin Elmer).
169 The crystal structures of the catalysts were analyzed by a Bruker advance D8 powder X-
170 ray diffraction (XRD) analyzer equipped with a Cu-Kα radiation (40 kV, 35 mA) at a scan
171 rate of 5 °/min. The spectra were scanned over a 2θ range from 5 to 90°. A Thermo Fisher

Nicolet iS5 Fourier Transformed Infrared (FTIR) spectrometer with a spectral resolution of 4 cm^{-1} was employed to characterize the functional groups of MC-SnO_x catalysts.

The ammonia-temperature-programmed desorption (NH_3-TPD) was employed to analyze acid properties of MC-SnO_x catalysts on a TP 5080 (Tianjin Xianquan) analyzer. Before adsorption of NH_3, the samples were treated at 450 °C for 30 min in the nitrogen atmosphere. Then catalysts were exposed to ammonia at 50 °C for 1 h and stabilized at the same temperature for 30 min before the run. Afterwards, the sample tube was heated to 500 °C at a rate of 10 °C/min. The desorption of NH_3 was detected by a thermal conductivity detector.

2.5. Product analysis

After separation of organic and water phase, furfural concentrations in organic phase were analyzed by a gas chromatograph (Shimadzu GC-2010 plus) equipped with a flame ionization detector (FID) and a HP-5ms column (30 m, 0.25 mm i.d., 0.25 μm film thickness). Nitrogen was used as the carrier gas with a flow rate of 1 mL/min. The injector was set at 240 °C and the detector was maintained at 250 °C. Initially, the column oven was maintained at 100 °C for 3 min, then the temperature was increase to 200 °C at a rate of 10 °C/min and kept for 10 min.

For samples of water phase, a HPLC (Agilent 1260) equipped with an Agilent Hi-plex H column (diameter 7.7 mm, length 300 mm, particle size 8 μm), a UV detector at a wavelength of 280 nm and a refractive index detector (RID) were employed to determine the concentrations of furfural and xylose. 5 mmol/L H_2SO_4 solution was used as mobile phase and the flow rate was 0.6 mL/min. The column oven and RID were maintained at 60 °C and 55 °C, respectively.

Furfural yield and selectivity contained furfural production in both water phase and organic phase. Furfural yield, D-xylose conversion and furfural selectivity were calculated by the following equations:

$$\text{Furfural yield}\ (\%) = \frac{\text{Moles of furfural in the product (mol)}}{\text{Moles of initial xylose (mol)}} \times 100 \quad (1)$$

$$\text{D}-\text{xylose conversion}\ (\%) = \frac{\text{Moles of xylose in reactant consumed (mol)}}{\text{Moles of initial xylose (mol)}} \times 100 \quad (2)$$

$$\text{Furfural selectivity}\ (\%) = \frac{\text{Moles of furfural in the product (mol)}}{\text{Moles of xylose in reactant consumed (mol)}} \times 100 \quad (3)$$

3. Results and discussion

3.1. Characterization of MC-SnO_x Catalyst

Table 1 and Fig. S2 shows surface area and pore volume properties of MC-SnO_x catalysts. The specific surface area increased gradually from 331.4 m^2/g to 387.4 m^2/g when annealing temperature rose from 400 to 500 °C, which can be attributed to improvement of higher annealing temperature. MC-SnO_x-400, has the lowest micropore surface area of

209 107.7 m^2/g and micropore volume of 47 cm^3/kg, which is only 41.5% and 43.9% of those
210 of MC-SnO_x-500. There are similar differences between MC-SnO_x-400 and MC-SnO_x-500
211 in other properties. It can be concluded that MC-SnO_x-400 has less micropore structure
212 and MC-SnO_x-500 has most, consistent with the measured pore distributions (Fig. S2).
213 MC-SnO_x-400 has abundant mesopore structure, leading to the largest average pore
214 diameter and the highest total pore volume among the catalysts.

Table 1

Surface areas and porosities of MC-SnO_x catalysts.

Catalyst Annealing temperature (°C)	S_{BET}[a] (m^2/g)	S_{micro}[b] (m^2/g)	V_{total}[c] (cm^3/kg)	V_{micro}[d] (cm^3/kg)	Average pore diameter (nm)
400	331.4	107.7	474	47	5.7
450	342.8	194.6	423	81	4.9
500	387.4	259.3	409	107	4.2
550	360.4	178.8	433	75	4.8
600	381.4	196.5	421	81	4.4

[a] Specific surface area calculated by Brunauer-Emmett-Teller (BET) equation.

[b] Specific surface area of micro-pores calculated by density functional theory (DFT) method.

[c] Total pore volume determined at P/P_0=0.99.

[d] Micropore volume calculated using t-plot method.

SEM images (see Fig. 2) demonstrate morphology and surface Sn proportion of MC-SnO_x catalysts. Fig. 2a, 2b, 2c, 2d and 2f captured irregular sharp particles of catalysts annealed at temperature from 400 °C to 600 °C. Ravine and pit structures were found on the surface of these catalyst particles. EDS mapping results indicate that MC-SnO_x-450 has the highest tin concentration on the surface of 5.31% (atomic ratio). With further increase of annealing temperature, the Sn content decreased sharply to MC-SnO_x-600 catalyst's 0.68%. However, another kind of globular particles are found in MC-SnO_x-600 (Fig. 2e). It can be noted that these particles had relatively smooth surface and very low levels of Sn content on their surface (only 0.02%). These globular particles were commonly found in MC-SnO_x-600 (Fig. S3). EDS mapping images (Fig. S4) proved that highly dispersed Sn species exist on the surface of catalysts' particles, which confirms successful hybridization of Sn species with MC in the catalysts.

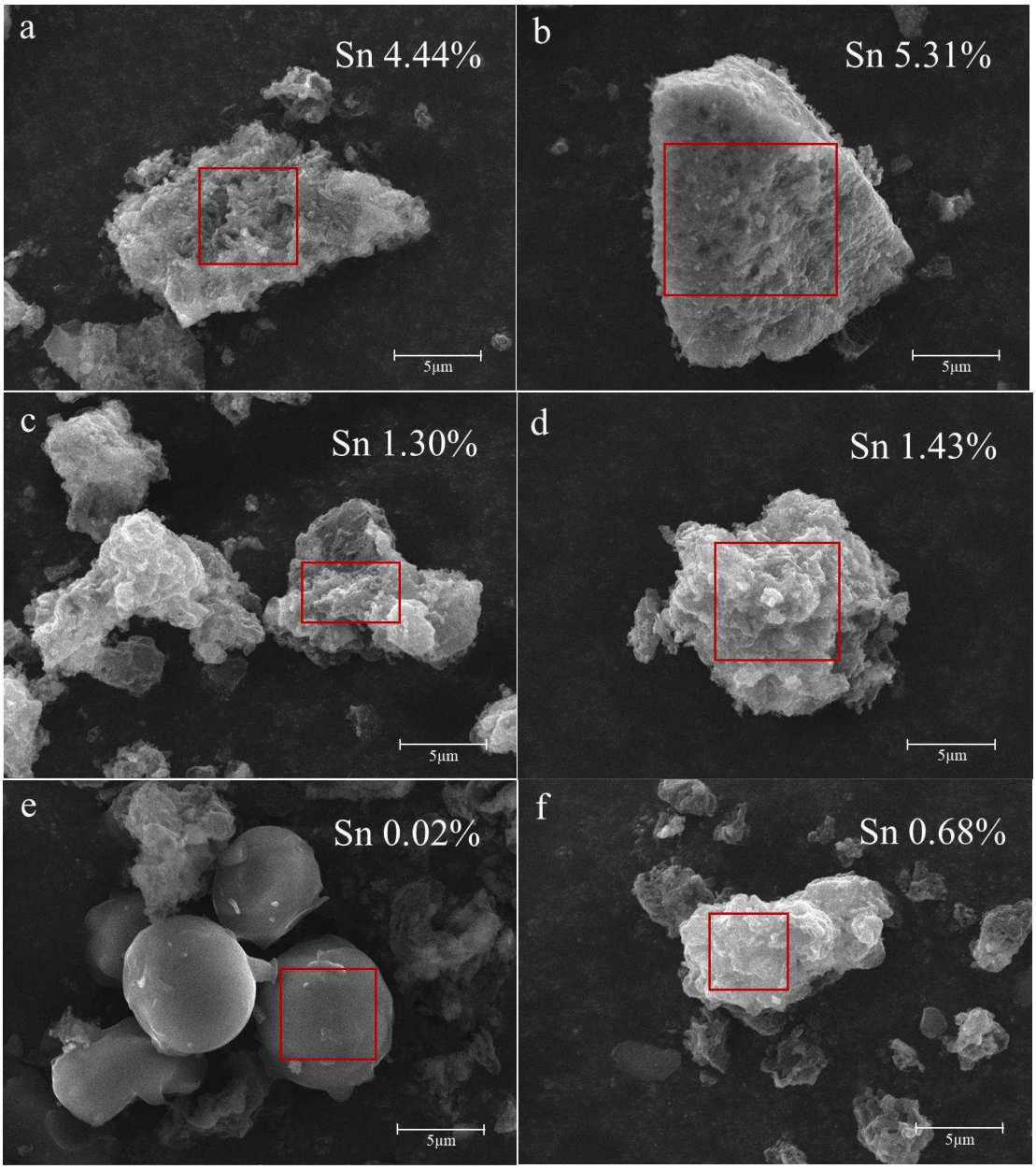

228 **Fig. 2.** SEM images and EDS mapping results of particles of (a) MC-SnO_x-400, (b) MC-

229 SnO_x-450, (c) MC-SnO_x-500, (d) MC-SnO_x-550, (e) globular MC-SnO_x-600, and (f)

230 irregular MC-SnO_x-600. Sn element content information (atomic ratio) was achieved by

231 EDS mapping of the area that framed in red boxes.

232

The X-ray photoelectron spectroscopy characterization of Sn in the catalysts is shown in Fig. 3. The fitting curves consist of three subpeaks in the XPS spectra of Sn $3d_{5/2}$. The resolved peaks at binding energies of ~485.6 eV, ~487.0 eV, ~487.8 eV originate from the Sn^0, Sn^{2+} and Sn^{4+} states, respectively. However, the binding energies for all peaks of Sn appear higher than the reference values (Quackenbush et al., 2013; Zhu et al., 2016). The increase of binding energies is probably caused by strong interactions between Sn species and the carbon-based support (Ma et al., 2011). MC-SnO_x catalyst annealed at 400 °C, has 10.60% Sn^0, 42.50% Sn^{2+} and 46.89% Sn^{4+} species. When the annealing temperature rose to 600 °C, there remained only 29.93% Sn^{4+} and the proportion of Sn^0 increased to 30.79%. It can be concluded that more Sn converted to lower valence species such as Sn^0 and Sn^{2+} at higher annealing temperature, which indicates that reduction reactions become more significant with increasing annealing temperature.

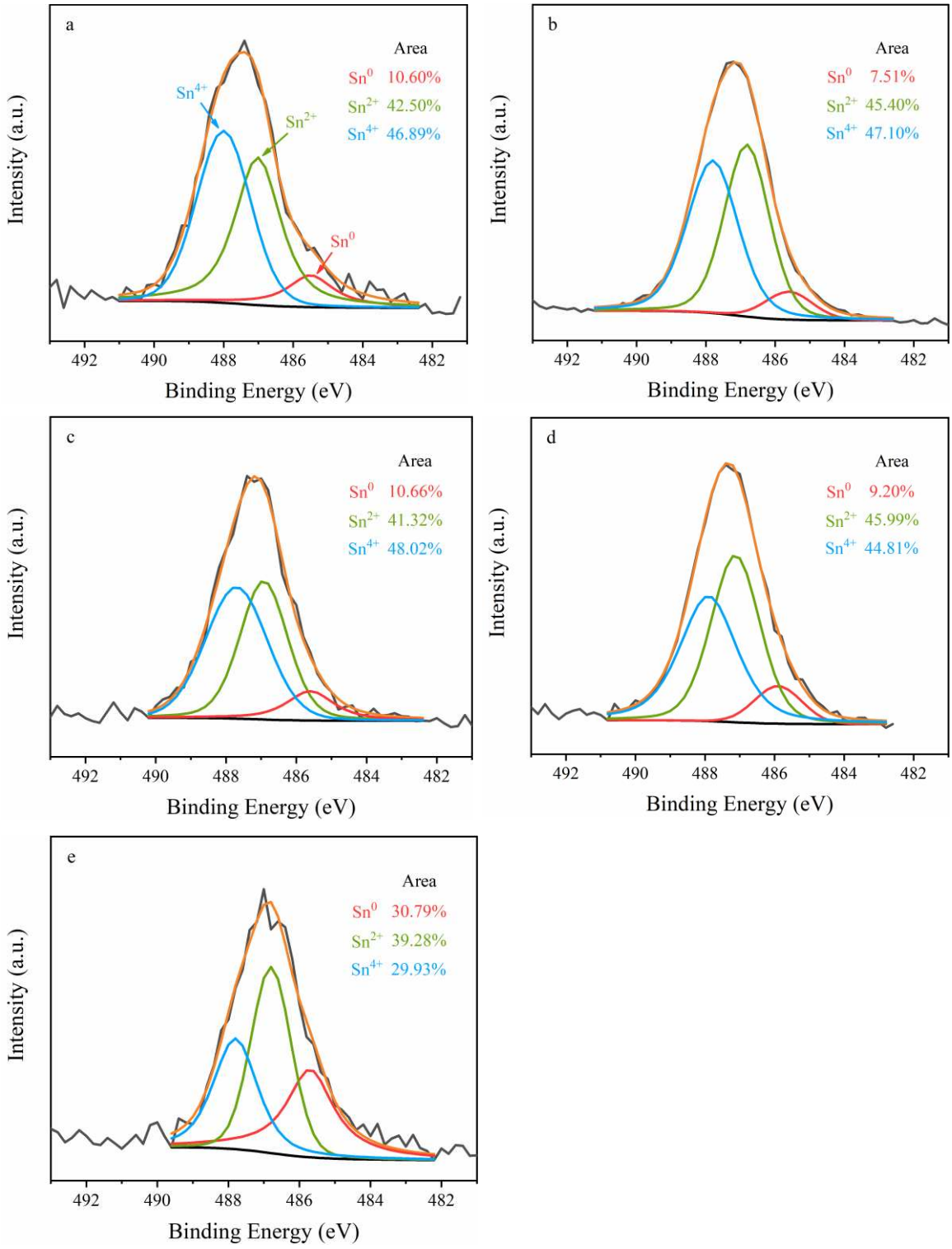

245 **Fig. 3.** X-ray photoelectron spectroscopy (XPS) Sn $3d_{5/2}$ spectra of (a) MC-SnO_x-400, (b)

246 MC-SnO_x-450, (c) MC-SnO_x-500, (d) MC-SnO_x-550, (e) MC-SnO_x-600 catalysts.

MC-SnO_x catalysts' XRD patterns were shown as Fig. 4. Peaks of tin dioxide can be found in all samples, which proved SnO_2 synthesis in the catalysts after annealing (Bellayer et al., 2009). For catalysts that were annealed at 550 °C and 600 °C, more peaks of metallic Sn appeared. The formation of metallic Sn was more significant in MC-SnO_x-600 than MC-SnO_x-550, suggesting that reduction reaction of Sn species became more intense when annealing at 600 °C. This result is in accordance with that of XPS analysis (see Fig. 2). Table S1 shows average crystallite sizes calculated by Scherrer formula. Both metallic Sn and tin dioxide grew larger in size with increasing annealing temperature.

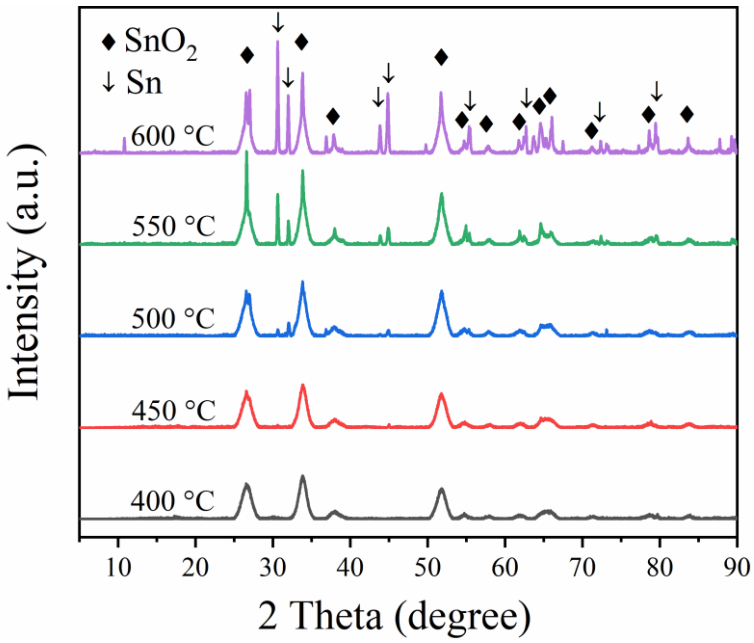

Fig. 4. X-Ray diffraction (XRD) pattern of MC-SnO_x catalysts.

NH_3-TPD was employed to analyze acid site strength and distribution in the catalysts. Fig. S5 depicts NH_3 desorption profile of MC-SnO_x catalysts. The distribution of acid site

was determined by NH_3 desorption temperature. In general, NH_3 peaks below 250 °C represent desorption of partially ionic NH_4^+ species which are absorbed by weak Brønsted acid sites on catalysts, while desorption peaks between 250 °C and 500 °C are caused by strong Brønsted acid sites and coordinated NH_3 bound Lewis acid sites, which are both considered as strong acid sites (Zhang et al., 2019; Zhao et al., 2016). Due to the limitations of catalyst annealing and pretreatment temperature, strong acid sites were calculated and compared based on peaks between 250 °C and 450 °C. Fig. 5 displays calculated acid site concentration of the catalysts. Total acid site concentration rose from 0.43 mmol/g to 0.45 mmol/g when annealing temperature increased from 400 °C to 450 °C. Further increasing of annealing temperature caused acid site concentration to come down quickly. When preparing the catalyst at 600 °C, acid site concentration remained only 33% of that in MC-SnO_x-450.

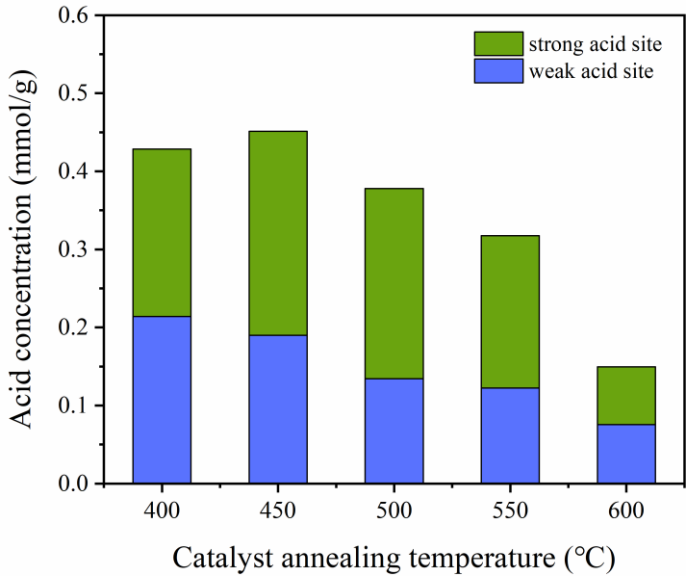

Fig. 5. Acid concentration of MC-SnO_x catalysts calculated from NH_3-TPD profiles.

3.2. Impact of annealing temperature on catalyst characteristics

Since the MC-SnO_x catalysts synthesis consists of two steps: (1) hydrothermal treatment to produce catalyst precursor containing Sn element; and (2) annealing preparation at different temperature to obtain activated MC-SnO_x catalyst, the key step that significantly influence the catalytic effect was step (2).

The difference of acid site abundance is induced by the tin species distribution and content variation. Increasing the annealing temperature can accelerate the reduction reaction of tin oxide. This reduction reaction was probably caused by reducing ambient CO produced in the high-temperature reaction of carbon-rich support. Fig. S6 demonstrates an oxygen-containing functional groups decrease with increasing annealing temperature, indicating the emission of CO or CO_2 could form a reducing atmosphere at higher temperature. In the metallurgical industry, iron concentrate is roasted in an atmosphere of CO and CO_2 to remove tin element and this process is called selective reduction volatilization (G. Li et al., 2014; Su et al., 2016), which has similar conditions with that in the annealing process in catalyst preparation. Thus, it is supposed that similar reduction and volatilization of Sn species happen in the annealing process, which follows the results of XPS and EDS. With an increase of annealing temperature, Sn^{4+} species react with reductive substance like C and CO produced during annealing process (Ma et al., 2011) and transform into lower valence species such as Sn^0 and Sn^{2+}. Lower valence Sn species

291 are further volatilized and cause decreases of surface Sn content. Similar reduction reaction
292 between tin oxide and carbon-based support in the annealing process were found in the
293 catalyst preparation for glucose isomerization reaction (Yang et al., 2020, 2019) and
294 conversion of cellulose into acetol (Liu et al., 2019). According to the mechanism of xylose
295 conversion into furfural mentioned in section 1, the amount of acid sites plays a dominant
296 role in influencing the conversion of xylose to furfural. The variation of Sn content and
297 valence further change the acid sites of catalysts and finally influence catalytic
298 performance of them.

299 It is worth noting that similar reduction reactions can occur in the preparation of other
300 carbon-supported metallic oxide catalyst. The changes of metal valence and volatilization
301 of low boiling point metal compounds should be considered when performing catalytic
302 reactions.

303

304 *3.3. Effect of MC-SnO_x catalyst annealing temperature on catalytic conversion*

305 The catalytic effect on furfural production from xylose of MC-SnO_x annealed at different
306 temperatures was evaluated in the batch reactor at 170 °C with a reaction time of 30 min
307 and summarized in Fig. 6. The addition of MC-SnO_x catalysts annealed at 400 to 550 °C
308 showed acceptable catalytic effect. When adding 0.15 g MC-SnO_x-400 in the reaction, the
309 highest furfural yield of 41.6% was reached, which corresponded to an increase of 18.8%

compared with the control group. MC-SnO_x-400 and MC-SnO_x-500 gave furfural yields of 39.6% and 38.1% respectively. While annealing temperature was further increased above 450 °C, the furfural yield went down. In the reaction with 0.15 g MC-SnO_x-600, the furfural yield was only 6.2% and inferior to that of the control group, indicating its negative effect in the reaction. In these six reaction groups, xylose conversions were always higher than 94.9%, which made furfural selectivity have similar trend with furfural yield. Formation of humins or other intermediates causes that the xylose cannot converted completely into furfural (Qing et al., 2017; Sweygers et al., 2020).

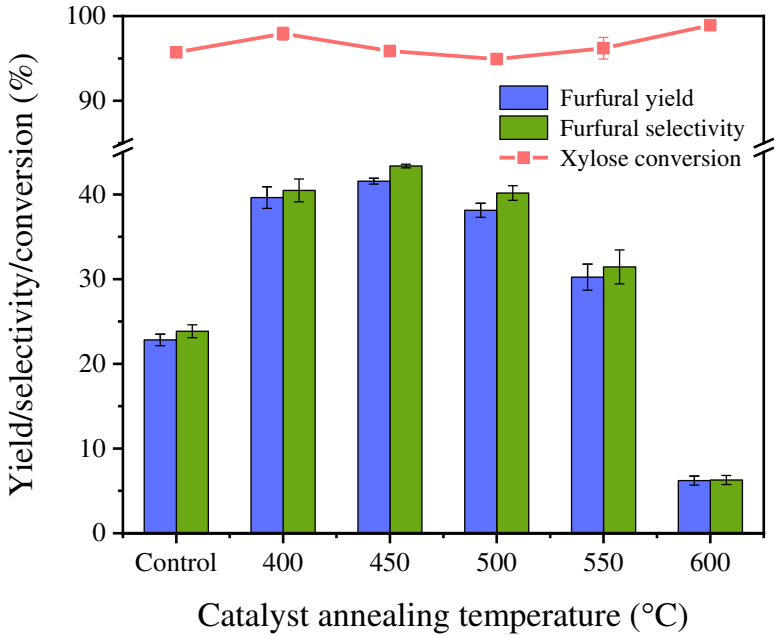

Fig. 6. Influence of annealing temperature (400 to 600 °C) of MC-SnO_x catalyst on catalytic conversion. Batches were conducted at 170 °C for 30 min with 0.15 g MC-SnO_x

320 catalyst (Control group contained no MC-SnO_x catalyst.) in 1:1 (v/v) 20 g/L xylose
321 aqueous phase/2-MTHF phase.
322
323 As the results showed in Fig. 5 and Fig. 6, trends of acid site concentration characterized
324 by NH_3-TPD and catalytic effect represented by furfural yield are very similar. Thus, the
325 catalytic effect difference can be ascribed to the different intensity of acid site
326 concentration. MC-SnO_x catalysts with higher acid site concentration have better catalytic
327 capability in the conversion of xylose to furfural, consistent with previous reports
328 (Chatterjee et al., 2019; Lin et al., 2017). Combining with the results of EDS Sn element
329 content and XPS Sn distribution, it was indicated that MC-SnO_x-400 and MC-SnO_x-450
330 had similar Sn species distribution, but extra surface Sn content can lead to a higher acid
331 concentration and catalytic effect for MC-SnO_x-450. MC-SnO_x-500 and MC-SnO_x-550
332 showed little difference in surface Sn content. However, MC-SnO_x-500 had both more Sn^{4+}
333 species and better catalytic effects, which demonstrate the higher catalytic activity of Sn^{4+}.
334 Further increasing annealing temperature induced the greatest amount of Sn^0 species and
335 the lowest catalytic effect of MC-SnOx-600. These results probably indicate a catalytic
336 activity order of $Sn^{4+} > Sn^{2+} > Sn^0$ in the reaction of xylose to furfural. To conclude, the
337 difference in both Sn content and Sn species distribution influences the acid site abundance

and finally causes the variation of catalytic effect. Fig. 7 shows the probable Sn transformation in MC-SnO_x catalysts.

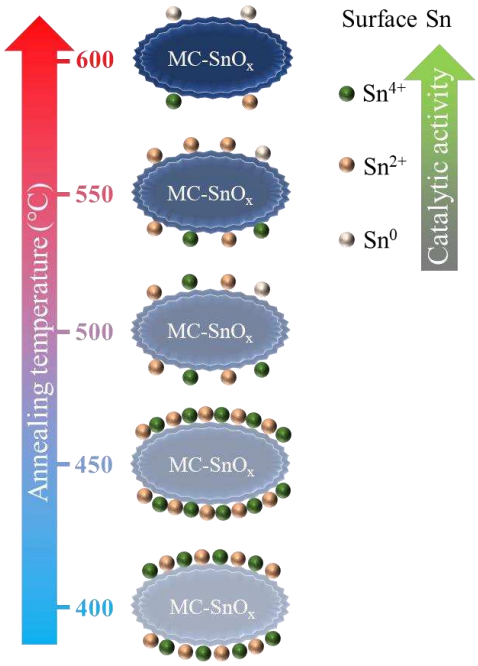

Fig. 7. Transformation schematic diagram of MC-SnO_x catalysts.

Morphology and microstructure changes further explain the catalytic effect variation. XRD results (see Fig. 4) prove the formation of metallic Sn in MC-SnO_x annealed higher than 500 °C. At the same time, crystallite dimension of both SnO_2 and Sn grew larger with the increase of annealing temperature (see Table S1). The growth of crystallite dimension means that the distribution of Sn species becomes concentrated, which can diminish the effective contact area of the catalysts.

3.4. Effect of MC-SnO_x catalyst loading on catalytic conversion

To analyze the impact of catalyst loading on the reaction of xylose to furfural, different catalyst amounts (0.05 g, 0.1 g, 0.15 g, 0.2 g and 0.3 g) of MC-SnO_x-450 catalyst were selected for reactions at 170 °C for 30 min. Fig. 8 showed that catalyst loading influenced the furfural yield, selectivity and xylose conversion. When adding 0.15 g of MC-SnO_x-450 catalyst, the reaction reached a highest furfural yield of 41.6% at a catalyst loading of 0.15 g. However, a further increase of catalyst loading above 0.15 g did not lead to a higher furfural yield. At the same time, the xylose conversion was improved gradually with increasing catalyst loading. Trends were recognized in furfural selectivity, whereby batches with more than 0.1 g catalyst were observed to increase xylose conversion. However, furfural yields were in growth in low catalyst loading and decreased in higher catalyst loading.

Excess catalyst loading may cause more side reactions, hence a decreased furfural yield and an increased xylose conversion simultaneously. Humins by-products may formed by the reaction between furfural and other intermediates in the presence of excess catalyst (Sweygers et al., 2020; Zhang et al., 2017). As seen in Fig. 8, the furfural yield using 0.15 g catalyst loading was only slightly higher than that using 0.1 g catalyst. Thus, a catalyst loading of 0.1 g was chosen in the following sections.

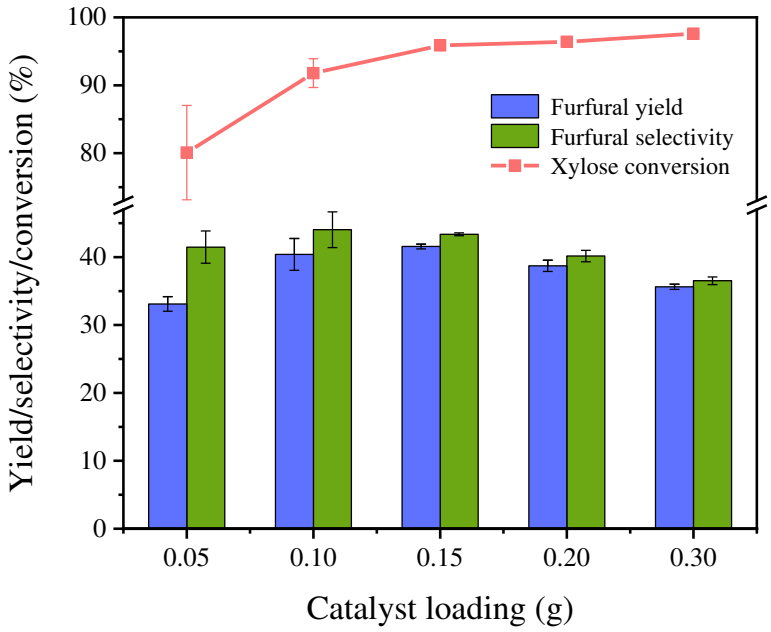

Fig. 8. Influence of MC-SnO_x-450 catalyst loading on catalytic conversion. Batches were conducted at 170 °C for 30 min with 0.05-0.3 g MC-SnO_x-450 catalyst in 1:1 (v/v) 20 g/L xylose aqueous phase/2-MTHF phase.

3.5. Synergistic effect of MC-SnO_x and NaCl catalyst

To study the catalytic effect of the MC-SnO_x catalyst in the presence of NaCl, amount of 0.2 mol/L, 0.5 mol/L, 1 mol/L and 2 mol/L NaCl were added into the aqueous solution, and the reactions were conducted at 170 °C for 30 min with or without 0.1 g MC-SnO_x-450 catalyst in each batch. The highest furfural yield of 57.9% was achieved when adding 2 mol/L NaCl and 0.1 g MC-SnO_x-450 catalyst in the reaction (Fig. 9). For batches adding both MC-SnO_x-450 catalyst and NaCl, furfural yield and furfural selectivity rose gradually with the increase of NaCl from 0 to 2 mol/L, which is in accordance with literature results (Delbecq et al., 2018; Le Guenic et al., 2016).

Another two groups of experiments were done without addition of the MC-SnO_x-450 catalyst. Adding more NaCl can improve the furfural selectivity as shown in Fig. 9. While comparing two groups of data of adding 0.2 mol/L NaCl with MC-SnO_x-450 catalyst and without MC-SnO_x-450 catalyst and adding 2 mol/L NaCl with MC-SnO_x-450 catalyst and without MC-SnO_x-450 catalyst, it can be found that 0.1g MC-SnO_x-450 catalyst contributed to the furfural yield by 20.4% and 23.7%, respectively. These results were a little higher than those batches only with 0.1 g MC-SnO_x-450 catalyst (furfural yield contribution of 17.6% showed in Fig. 8), which can be ascribed to the improvement of salting out effect (Román-Leshkov et al., 2007; Sweygers et al., 2021). It proved that MC-

391 SnO_x catalyst and NaCl have a synergistic catalytic effect in conversion from xylose to
392 furfural.

393 However, contribution of furfural yield by adding more NaCl from 0.2 mol/L to 2 mol/L
394 was only 7.7% and 0.2 mol/L NaCl itself improved furfural yield by 9.7%, which means
395 that it is not economical to multiple NaCl concentration by 10 times. These results prove
396 low concentration of NaCl to be effective and economical in conversion of xylose into
397 furfural. In addition, the intense concentration of chlorine salt can cause severe corrosion
398 of reactors and refractory wastewater pollution containing high concentration of salt. To
399 balance the furfural yield and other factors, a NaCl concentration of 0.2 mol/L was selected
400 to complete next part's experiments. At the same time, since seawater contains about 0.5
401 mol/L NaCl, these results indicate the potential of applying seawater (Mao et al., 2013) or
402 wastewater containing NaCl as a low cost reaction solvent and NaCl catalyst source in
403 conversion of xylose to furfural.

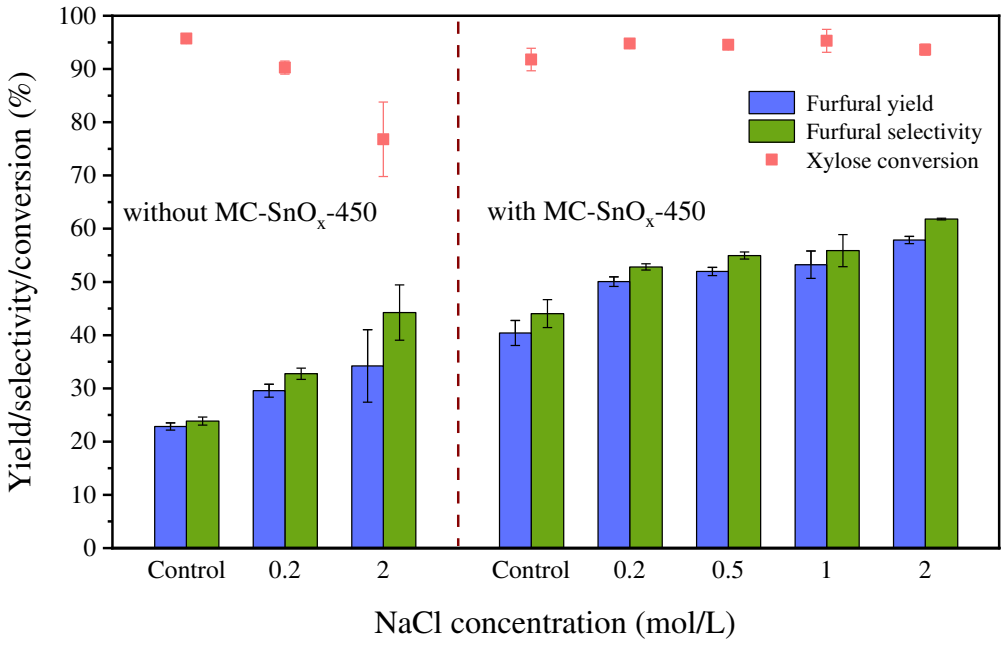

404 **Fig. 9.** Catalytic effect of NaCl in the system and synergistic effect between MC-SnO_x and
405 NaCl. 0 mol/L (control groups), 0.2 mol/L, 0.5 mol/L, 1 mol/L and 2 mol/L NaCl were
406 added into 1:1 (v/v) 20 g/L xylose aqueous phase/2-MTHF phase and reacted at 170 °C for
407 30 min. Groups in right half contained 0.1 g MC-SnO_x-450 catalysts.

408

409 *3.6. Effect of reaction temperature and time on catalytic conversion*

410 In Fig. 10, the influence of reaction temperature and time was investigated (160–180 °C
411 and 10–120 min). Each batch contains 0.2 mol/L NaCl in aqueous phase and 0.1 g MC-
412 SnO_x-450 catalyst. The highest furfural yield of 54.8% was reached at 180 °C for 40 min.
413 However, the batches at 180 °C for 20 and 30 min had a very close furfural yield at 53.9%
414 and 54.6%, which suggested that the reaction at 180 °C for 20 min is suitable for furfural

415 production. For all reaction temperature, furfural yield reached peak at certain reaction time
416 (40 min for 180 °C, 60 min for 170 °C and 100 min for 160 °C). As shown in Fig. 10, low
417 reaction temperature reaction needs more time to reach the highest furfural yield. At the
418 same time, the highest furfural yields were 50.0%, 53.0% and 54.8% for reaction at 160 °C,
419 170 °C and 180 °C, which proves reaction at 180 °C can achieve better furfural yield than
420 that at 160 °C and 170 °C in a shorter time. Higher temperature of 180 °C can accelerate
421 the reaction greatly comparing to the lower temperature of 170 °C and 160 °C, which save
422 time and possibly energy for reaction batches. A similar pattern was found for xylose
423 conversion. With the increase of reaction temperature, the furfural yields first increased
424 then decreased after reacting for more than 40 min at 180 °C, as excess reaction time can
425 cause furfural degradation and limits furfural yield. Similar phenomena were observed for
426 batches at 160 °C and 170 °C.

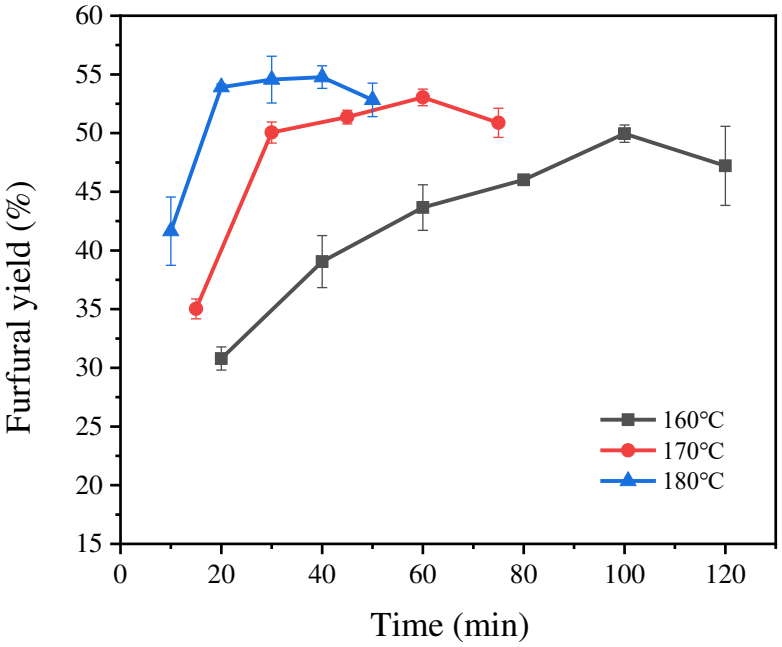
Furfural yield (%)
Time (min)
160°C
170°C
180°C

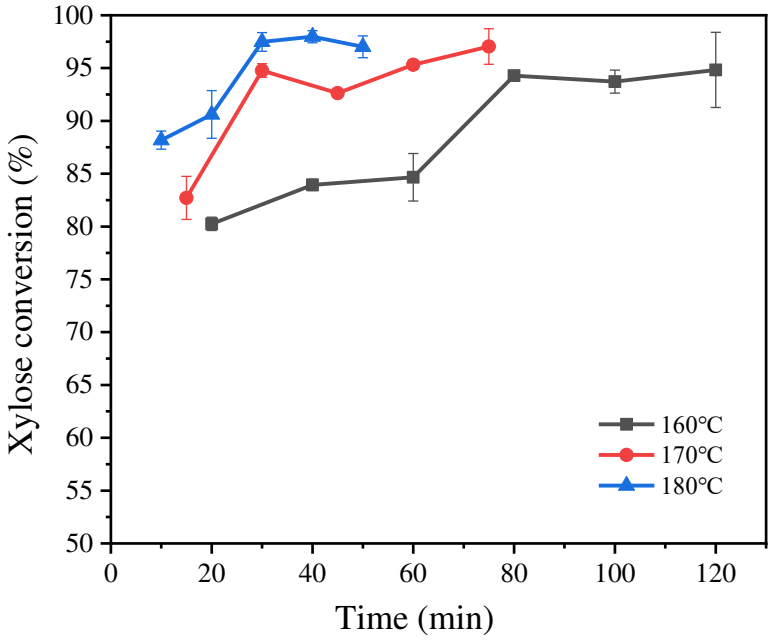
Xylose conversion (%)
Time (min)
160°C
170°C
180°C

427

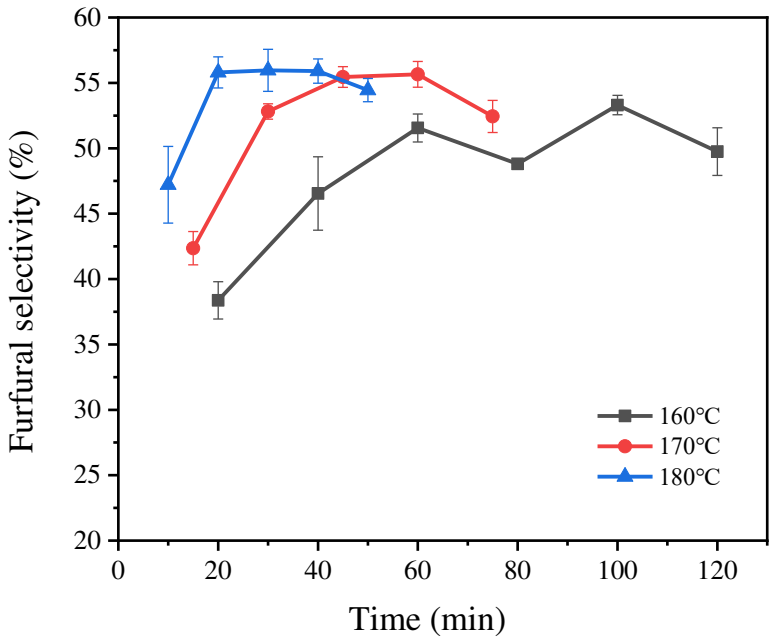

Fig. 10. Influence of reaction temperature and time on catalytic conversion. Batches were conducted at 160–180 °C for 10–120 min with 0.1 g MC-SnO_x-450 catalyst in 1:1 (v/v) 20 g/L xylose and 0.2 mol/L NaCl aqueous phase/2-MTHF phase.

3.7. Reusability of MC-SnO_x catalyst in the system

The reusability is critical to catalyst's application in the industrial production process. Fig. 11 showed results of MC-SnO_x catalyst's reusability in 5 times' recycle. The MC-SnO_x-450 catalyst was separated and washed by pure water and ethanol for several times to remove residues after each batch. The results demonstrate that MC-SnO_x-450 catalyst has a good reusability. The furfural yield went down from first run's 53.9% to third run's

48.6%, which caused only 9.8% total catalytic performance decrease (calculated by furfural production). After 3 times' run, furfural yield maintained stable and kept higher than 48.2%, which proofs that MC-SnO_x catalyst can maintain a stable catalytic performance in the following run. Xylose conversion rate also first decreased from first run to third run and then kept stable. Comparing with other catalysts such as sulfonated carbon based catalysts (Deng et al., 2016), SO_4^{2-}/SnO_2^- MMT (Qing et al., 2017), Sn-MMT (Li et al., 2015) and SO_4^{2-}/SnO_2-AI_2O_3-CFA (Gong et al., 2019), MC-SnO_x catalyst showed prior reusability without regeneration. The trend that catalytic performance decreased slightly from first run to third run and maintained stable in the following run indicates promising application potential of MC-SnO_x catalyst.

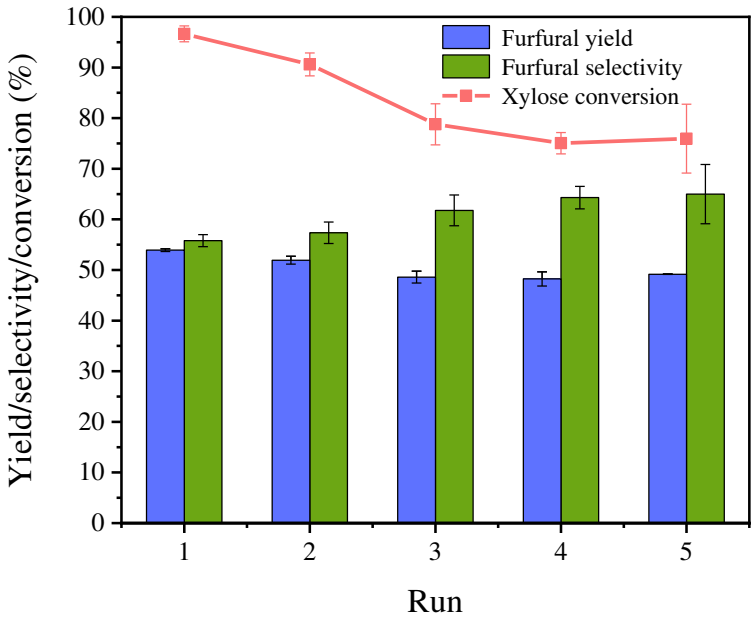

Fig. 11. Reusability of MC-SnO_x-450 catalyst for conversion xylose into furfural. Batches were conducted at 180 °C for 20 min with 0.1 g MC-SnO_x-450 catalyst in 1:1 (v/v) 20 g/L xylose and 0.2 mol/L NaCl aqueous phase/2-MTHF phase.

4. Conclusions

We produced a novel MC-SnO_x catalyst without acid treatment process to convert xylose into furfural. In the preparation process, annealing temperature impacted most on catalytic performance because higher temperature can cause decrease of surface Sn content and promote reduction reaction, volatilization and aggregation of Sn species, which finally influenced acid site concentration of catalysts and limited furfural yield. The best annealing temperature was 450 °C. A reasonable furfural yield of 53.9% was achieved using the

conditions of 0.1g MC-SnO_x-450 in 20 g/L xylose aqueous phase with 0.2 mol/L NaCl in the reaction at 180 °C for 20 min representing a balance between catalytic performance, cost, equipment safety and environmental concerns. The synergistic catalytic effect was found between MC-SnO_x and NaCl and effectivity of low concentration of NaCl indicate the potential of applying seawater or wastewater containing NaCl as a low-cost reaction solvent and NaCl catalyst source in conversion of xylose to furfural. In addition, MC-SnO_x catalyst displayed a good reusability. These results guide the further development of carbon-supported tin oxide catalysts in furfural production.

Acknowledgements

This research was supported by the National Key Research and Development Program of China (No. 2017YFC0212205), the National Natural Science Foundation of China (No. 21876030), the International Cooperation Project of Science and Technology Commission of Shanghai Municipality (No. 18230710700).

Appendix A. Supplementary data

E-supplementary data of this work can be found in online version of the paper.

References

Agirrezabal-Telleria, I., Larreategui, A., Requies, J., Güemez, M.B., Arias, P.L., 2011. Furfural production from xylose using sulfonic ion-exchange resins (Amberlyst) and simultaneous stripping with nitrogen. Bioresour. Technol. 102, 7478–7485. https://doi.org/10.1016/j.biortech.2011.05.015

Agirrezabal-Telleria, I., Requies, J., Güemez, M.B., Arias, P.L., 2012. Furfural production from xylose + glucose feedings and simultaneous N2-stripping. Green Chem. 14, 3132–3140. https://doi.org/10.1039/c2gc36092f

Bellayer, S., Viau, L., Tebby, Z., Toupance, T., Bideau, J. Le, Vioux, A., 2009. Immobilization of ionic liquids in translucent tin dioxide monoliths by sol–gel processing. Dalt. Trans. 1307–1313. https://doi.org/10.1039/b814978j

Bhaumik, P., Dhepe, P.L., 2016. Solid acid catalyzed synthesis of furans from carbohydrates. Catal. Rev. 58, 36–112. https://doi.org/10.1080/01614940.2015.1099894

Cai, C.M., Zhang, T., Kumar, R., Wyman, C.E., 2014. Integrated furfural production as a renewable fuel and chemical platform from lignocellulosic biomass. J. Chem. Technol. Biotechnol. 89, 2–10. https://doi.org/10.1002/jctb.4168

Chatterjee, A., HU, X., Lam, F.L.Y., 2019. Modified coal fly ash waste as an efficient heterogeneous catalyst for dehydration of xylose to furfural in biphasic medium. Fuel 239, 726–736. https://doi.org/10.1016/j.fuel.2018.10.138

Choudhary, V., Sandler, S.I., Vlachos, D.G., 2012. Conversion of xylose to furfural using Lewis and Brønsted acid catalysts in aqueous media. ACS Catal. 2, 2022–2028. https://doi.org/10.1021/cs300265d

Delbecq, F., Takahashi, Y., Kondo, T., Corbas, C.C., Ramos, E.R., Len, C., 2018. Microwave assisted efficient furfural production using nano-sized surface-sulfonated diamond powder. Catal. Commun. 110, 74–78. https://doi.org/10.1016/j.catcom.2018.03.020

Deng, A., Lin, Q., Yan, Y., Li, H., Ren, J., Liu, C., Sun, R., 2016. A feasible process for furfural production from the pre-hydrolysis liquor of corncob via biochar catalysts in a new biphasic system. Bioresour. Technol. 216, 754–760. https://doi.org/10.1016/j.biortech.2016.06.002

Enslow, K.R., Bell, A.T., 2015. The role of metal halides in enhancing the dehydration of xylose to furfural. ChemCatChem 7, 479–489. https://doi.org/10.1002/cctc.201402842

Gong, L., Xu, Z.Y., Dong, J.J., Li, H., Han, R.Z., Xu, G.C., Ni, Y., 2019. Composite coal fly ash solid acid catalyst in synergy with chloride for biphasic preparation of

514 furfural from corn stover hydrolysate. Bioresour. Technol. 293, 122065.
515 https://doi.org/10.1016/j.biortech.2019.122065
516 Guenic, S. Le, Delbecq, F., Ceballos, C., Len, C., 2015. Microwave-assisted dehydration
517 of D-xylose into furfural by diluted inexpensive inorganic salts solution in a biphasic
518 system. J. Mol. Catal. A Chem. 410, 1–7.
519 https://doi.org/10.1016/j.molcata.2015.08.019
520 Guo, T., Li, X., Liu, X., Guo, Y., Wang, Y., 2018. Catalytic Transformation of
521 Lignocellulosic Biomass into Arenes, 5-Hydroxymethylfurfural, and Furfural.
522 ChemSusChem 11, 2758–2765. https://doi.org/10.1002/cssc.201800967
523 Guo, X., Guo, F., Li, Y., Zheng, Z., Xing, Z., Zhu, Z., Liu, T., Zhang, X., Jin, Y., 2018.
524 Dehydration of D-xylose into furfural over bimetallic salts of heteropolyacid in
525 DMSO/H2O mixture. Appl. Catal. A Gen. 558, 18–25.
526 https://doi.org/10.1016/j.apcata.2018.03.027
527 Gupta, N.K., Fukuoka, A., Nakajima, K., 2017. Amorphous Nb2O5 as a Selective and
528 Reusable Catalyst for Furfural Production from Xylose in Biphasic Water and
529 Toluene. ACS Catal. 7, 2430–2436. https://doi.org/10.1021/acscatal.6b03682
530 Jiang, C.X., Di, J.H., Su, C., Yang, S.Y., Ma, C.L., He, Y.C., 2018. One-pot co-catalysis
531 of corncob with dilute hydrochloric acid and tin-based solid acid for the

532 enhancement of furfural production. Bioresour. Technol. 268, 315–322.
533 https://doi.org/10.1016/j.biortech.2018.07.147
534 Karinen, R., Vilonen, K., Niemelä, M., 2011. Biorefining: Heterogeneously catalyzed
535 reactions of carbohydrates for the production of furfural and hydroxymethylfurfural.
536 ChemSusChem 4, 1002–1016. https://doi.org/10.1002/cssc.201000375
537 Le Guenic, S., Gergela, D., Ceballos, C., Delbecq, F., Len, C., 2016. Furfural production
538 from D-xylose and xylan by using stable nafion NR50 and NaCl in a microwave-
539 assisted biphasic reaction. Molecules 21, 1102.
540 https://doi.org/10.3390/molecules21081102
541 Li, G., You, Z., Zhang, Y., Rao, M., Wen, P., Guo, Y., Jiang, T., 2014. Synchronous
542 Volatilization of Sn, Zn, and As, and Preparation of Direct Reduction Iron (DRI)
543 from a Complex Iron Concentrate via CO Reduction. Jom 66, 1701–1710.
544 https://doi.org/10.1007/s11837-013-0852-4
545 Li, H., Deng, A., Ren, J., Liu, C., Wang, W., Peng, F., Sun, R., 2014. A modified
546 biphasic system for the dehydration of d-xylose into furfural using SO42-/TiO2-
547 ZrO2/La3+ as a solid catalyst. Catal. Today 234, 251–256.
548 https://doi.org/10.1016/j.cattod.2013.12.043
549 Li, H., Ren, J., Zhong, L., Sun, R., Liang, L., 2015. Production of furfural from xylose,
550 water-insoluble hemicelluloses and water-soluble fraction of corncob via a tin-

loaded montmorillonite solid acid catalyst. Bioresour. Technol. 176, 242–248. https://doi.org/10.1016/j.biortech.2014.11.044

Li, X.K., Fang, Z., Luo, J., Su, T.C., 2016. Coproduction of Furfural and Easily Hydrolyzable Residue from Sugar Cane Bagasse in the MTHF/Aqueous Biphasic System: Influence of Acid Species, NaCl Addition, and MTHF. ACS Sustain. Chem. Eng. 4, 5804–5813. https://doi.org/10.1021/acssuschemeng.6b01847

Lin, Q., Li, H., Wang, X., Jian, L., Ren, J., Liu, C., Sun, R., 2017. SO42−/Sn-MMT solid acid catalyst for xylose and xylan conversion into furfural in the biphasic system. Catalysts 7, 1–14. https://doi.org/10.3390/catal7040118

Liu, Xiaohao, Liu, Xiaodong, Xu, G., Zhang, Y., Wang, C., Lu, Q., Ma, L., 2019. Highly efficient catalytic conversion of cellulose into acetol over Ni-Sn supported on nanosilica and the mechanism study. Green Chem. 21, 5647–5656. https://doi.org/10.1039/c9gc02449b

Ma, H., Teng, K., Fu, Y., Song, Y., Wang, Y., Dong, X., 2011. Synthesis of visible-light responsive Sn-SnO2/C photocatalyst by simple carbothermal reduction. Energy Environ. Sci. 4, 3067–3073. https://doi.org/10.1039/c1ee01095f

Mao, L., Zhang, L., Gao, N., Li, A., 2013. Seawater-based furfural production via corncob hydrolysis catalyzed by FeCl3 in acetic acid steam. Green Chem. 15, 727–737. https://doi.org/10.1039/c2gc36346a

570 Nimlos, M.R., Qian, X., Davis, M., Himmel, M.E., Johnson, D.K., 2006. Energetics of
571 xylose decomposition as determined using quantum mechanics modeling. J. Phys.
572 Chem. A 110, 11824–11838. https://doi.org/10.1021/jp0626770
573 Qing, Q., Guo, Q., Zhou, L., Wan, Y., Xu, Y., Ji, H., Gao, X., Zhang, Y., 2017. Catalytic
574 conversion of corncob and corncob pretreatment hydrolysate to furfural in a biphasic
575 system with addition of sodium chloride. Bioresour. Technol. 226, 247–254.
576 https://doi.org/10.1016/j.biortech.2016.11.118
577 Quackenbush, N.F., Allen, J.P., Scanlon, D.O., Sallis, S., Hewlett, J.A., Nandur, A.S.,
578 Chen, B., Smith, K.E., Weiland, C., Fischer, D.A., Woicik, J.C., White, B.E.,
579 Watson, G.W., Piper, L.F.J., 2013. Origin of the bipolar doping behavior of SnO
580 from X-ray spectroscopy and density functional theory. Chem. Mater. 25, 3114–
581 3123. https://doi.org/10.1021/cm401343a
582 Román-Leshkov, Y., Barrett, C.J., Liu, Z.Y., Dumesic, J.A., 2007. Production of
583 dimethylfuran for liquid fuels from biomass-derived carbohydrates. Nature 447,
584 982–985. https://doi.org/10.1038/nature05923
585 Su, Z., Zhang, Y., Liu, B., Zhou, Y., Jiang, T., Li, G., 2016. Reduction behavior of SnO2
586 in the tin-bearing iron concentrates under CO-CO2 atmosphere. Part I: Effect of
587 magnetite. Powder Technol. 292, 251–259.
588 https://doi.org/10.1016/j.powtec.2015.12.047

589 Sweygers, N., Depuydt, D.E.C., Willem, A., Vuure, V., Degrève, J., Potters, G., Dewil,
590 R., Appels, L., 2020. Simultaneous production of 5-hydroxymethylfurfural and
591 furfural from bamboo (Phyllostachys nigra “Boryana") in a biphasic reaction
592 system. Chem. Eng. J. 386, 123957. https://doi.org/10.1016/j.cej.2019.123957
593 Sweygers, N., Harrer, J., Dewil, R., Appels, L., 2018. A microwave-assisted process for
594 the in-situ production of 5-hydroxymethylfurfural and furfural from lignocellulosic
595 polysaccharides in a biphasic reaction system. J. Clean. Prod. 187, 1014–1024.
596 https://doi.org/10.1016/j.jclepro.2018.03.204
597 Sweygers, N., Mohammadreza, K., Aminabhavi, T.M., Dewil, R., Appels, L., 2021.
598 Efficient microwave-assisted production of furanics and hydrochar from bamboo
599 (Phyllostachys nigra “Boryana”) in a biphasic reaction system: effect of inorganic
600 salts. Biomass Convers. Biorefinery. https://doi.org/10.1007/s13399-021-01372-6
601 Teng, X., Si, Z., Li, S., Yang, Y., Wang, Z., Li, G., Zhao, J., Cai, D., Qin, P., 2020. Tin-
602 loaded sulfonated rape pollen for efficient catalytic production of furfural from corn
603 stover. Ind. Crops Prod. 151, 112481. https://doi.org/10.1016/j.indcrop.2020.112481
604 Vomstein, T., Grande, P.M., Leitner, W., Domínguezdemaría, P., 2011. Iron-catalyzed
605 furfural production in biobased biphasic systems: From pure sugars to direct use of
606 crude xylose effluents as feedstock. ChemSusChem 4, 1592–1594.
607 https://doi.org/10.1002/cssc.201100259

608 Wang, W., Ren, J., Li, H., Deng, A., Sun, R., 2015. Direct transformation of xylan-type
609 hemicelluloses to furfural via SnCl4 catalysts in aqueous and biphasic systems.
610 Bioresour. Technol. 183, 188–194. https://doi.org/10.1016/j.biortech.2015.02.068
611 Wang, X., Li, H., Lin, Q., Li, R., Li, W., Peng, F., Ren, J., 2019. Efficient catalytic
612 conversion of dilute-oxalic acid pretreated bagasse hydrolysate to furfural using
613 recyclable ironic phosphates catalysts. Bioresour. Technol. 290, 121764.
614 https://doi.org/10.1016/j.biortech.2019.121764
615 Wang, Y., Delbecq, F., Kwapinski, W., Len, C., 2017. Application of sulfonated carbon-
616 based catalyst for the furfural production from D-xylose and xylan in a microwave-
617 assisted biphasic reaction. Mol. Catal. 438, 167–172.
618 https://doi.org/10.1016/j.mcat.2017.05.031
619 Wettstein, S.G., Martin Alonso, D., Gürbüz, E.I., Dumesic, J.A., 2012. A roadmap for
620 conversion of lignocellulosic biomass to chemicals and fuels. Curr. Opin. Chem.
621 Eng. 1, 218–224. https://doi.org/10.1016/j.coche.2012.04.002
622 Yang, T., Zhou, Y.H., Zhu, S.Z., Pan, H., Huang, Y.B., 2017. Insight into Aluminum
623 Sulfate-Catalyzed Xylan Conversion into Furfural in a Γ-Valerolactone/Water
624 Biphasic Solvent under Microwave Conditions. ChemSusChem 10, 4066–4079.
625 https://doi.org/10.1002/cssc.201701290

626 Yang, X., Yu, I.K.M., Cho, D.W., Chen, S.S., Tsang, D.C.W., Shang, J., Yip, A.C.K.,
627 Wang, L., Ok, Y.S., 2019. Tin-Functionalized Wood Biochar as a Sustainable Solid
628 Catalyst for Glucose Isomerization in Biorefinery. ACS Sustain. Chem. Eng. 7,
629 4851–4860. https://doi.org/10.1021/acssuschemeng.8b05311
630 Yang, X., Yu, I.K.M., Tsang, D.C.W., Budarin, V.L., Clark, J.H., Wu, K.C.W., Yip,
631 A.C.K., Gao, B., Lam, S.S., Ok, Y.S., 2020. Ball-milled, solvent-free Sn-
632 functionalisation of wood waste biochar for sugar conversion in food waste
633 valorisation. J. Clean. Prod. 268, 122300.
634 https://doi.org/10.1016/j.jclepro.2020.122300
635 Zhang, C., Jia, C., Cao, Y., Yao, Y., Xie, S., Zhang, S., Lin, H., 2019. Water-assisted
636 selective hydrodeoxygenation of phenol to benzene over the Ru composite catalyst
637 in the biphasic process. Green Chem. 21, 1668–1679.
638 https://doi.org/10.1039/c8gc04017f
639 Zhang, L., Xi, G., Chen, Z., Jiang, D., Yu, H., Wang, X., 2017. Highly selective
640 conversion of glucose into furfural over modified zeolites. Chem. Eng. J. 307, 868–
641 876. https://doi.org/10.1016/j.cej.2016.09.001
642 Zhao, X., Huang, L., Namuangruk, S., Hu, H., Hu, X., Shi, L., Zhang, D., 2016.
643 Morphology-dependent performance of Zr-CeVO4/TiO2 for selective catalytic

reduction of NO with NH3. Catal. Sci. Technol. 6, 5543–5553. https://doi.org/10.1039/c6cy00326e

Zhu, H., Rosenfeld, D.C., Harb, M., Anjum, D.H., Hedhili, M.N., Ould-Chikh, S., Basset, J.M., 2016. Ni-M-O (M = Sn, Ti, W) Catalysts Prepared by a Dry Mixing Method for Oxidative Dehydrogenation of Ethane. ACS Catal. 6, 2852–2866. https://doi.org/10.1021/acscatal.6b00044